ACS APPLIED MATERIALS & INTERFACES

www.acsami.org

Research Article

Calcium Alginate as an Active Device Component for Light-Triggered Degradation of 2D MoS_2-Based Transient Electronics

Md Golam Kaium, Sang Sub Han, Chung Won Lee, and Yeonwoong Jung*

Cite This: *ACS Appl. Mater. Interfaces* 2024, 16, 39673−39682

Read Online

ACCESS | Metrics & More | Article Recommendations | Supporting Information

ABSTRACT: Transient electronics technology has enabled the programmed disintegration of functional devices, paving the way for environmentally sustainable management of electronic wastes as well as facilitating the exploration of novel device concepts. While a variety of inorganic and/or organic materials have been employed as media to introduce transient characteristics in electronic devices, they have been mainly limited to function as passive device components. Herein, we report that calcium (Ca) alginate, a natural biopolymer, exhibits multifunctionalities of introducing light-triggered transient characteristics as well as constituting active components in electronic devices integrated with two-dimensional (2D) molybdenum disulfide (MoS_2) layers. Ca^{2+} ions-based alginate electrolyte films are prepared through hydrolysis reactions and are subsequently incorporated with riboflavin, a natural photosensitizer, for the light-driven dissolution of 2D MoS_2 layers. The alginate films exhibit strain-sensitive triboelectricity, confirming the presence of abundant mobile Ca^{2+} ions, which enables them to be active components of 2D MoS_2 field-effect transistors (FETs) functioning as electrolyte top-gates. The alginate-integrated 2D MoS_2 FETs display intriguing transient characteristics of spontaneous degradation upon ultraviolet-to-visible light illumination as well as water exposure. Such transient characteristics are demonstrated even in ambient conditions with natural sunlight, highlighting the versatility of the developed approach. This study emphasizes a relatively unexplored aspect of combining naturally abundant polymers with emerging near atom-thickness semiconductors toward realizing unconventional and transformative device functionalities.

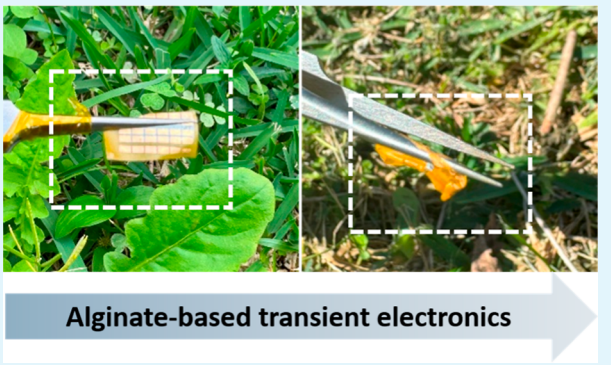

KEYWORDS: *calcium alginate, riboflavin, 2D MoS_2, light-triggered degradation, transient electronics, electrolyte-gated FET, green electronics*

INTRODUCTION

In due course, the concept of "transient electronics" emerged as an ideational response to the challenges posed by escalating nonrecyclable "electronic wastes" (i.e., discarded electronic devices) and its consequential adverse effects associated with conventional electronic device technologies.[1−3] At the end of their lifecycle, conventional electronic devices are typically consigned to landfills or subjected to chemical/combustion-based recovery processes aimed at recovering precious metals,[4] both of which, however, introduce environmental and health concerns.[5] Transient electronic devices share functional similarities with conventional electronics, but their certain device components with intrinsic biodegradability/compatibility allow them to disintegrate in a programmed manner, minimally releasing hazardous elements.[6,7] Furthermore, the emerging concept of transient electronics offers new opportunities for applications where conventional electronic devices fall short. Some examples include implantable devices with biocompatible degradability for medical applications[8,9] or self-destructive encryption devices with programmed security for mission-critical defense applications.[10,11] Extensive studies have been dedicated to identifying functional materials that can introduce transient characteristics into conventional devices as well as their associated integration methods. A number of organic or inorganic semiconducting materials have been explored in various structures,[12−14] which have recently expanded to near atom-thickness two-dimensional transition (2D) metal dichalcogenide layers, notably molybdenum disulfide (MoS_2), due to their unprecedented optoelectronic and mechanical properties.[15,16] Recent advancements in 2D MoS_2-based transition electronics have focused on fabricating devices on biodegradable substrates such as cellulose or poly(vinyl alcohol)[17] and demonstrating their disintegration in aqueous or pH-sensitive buffer solutions. However, in these approaches, challenges exist associated with controlling the

Received: June 5, 2024
Revised: July 9, 2024
Accepted: July 15, 2024
Published: July 18, 2024

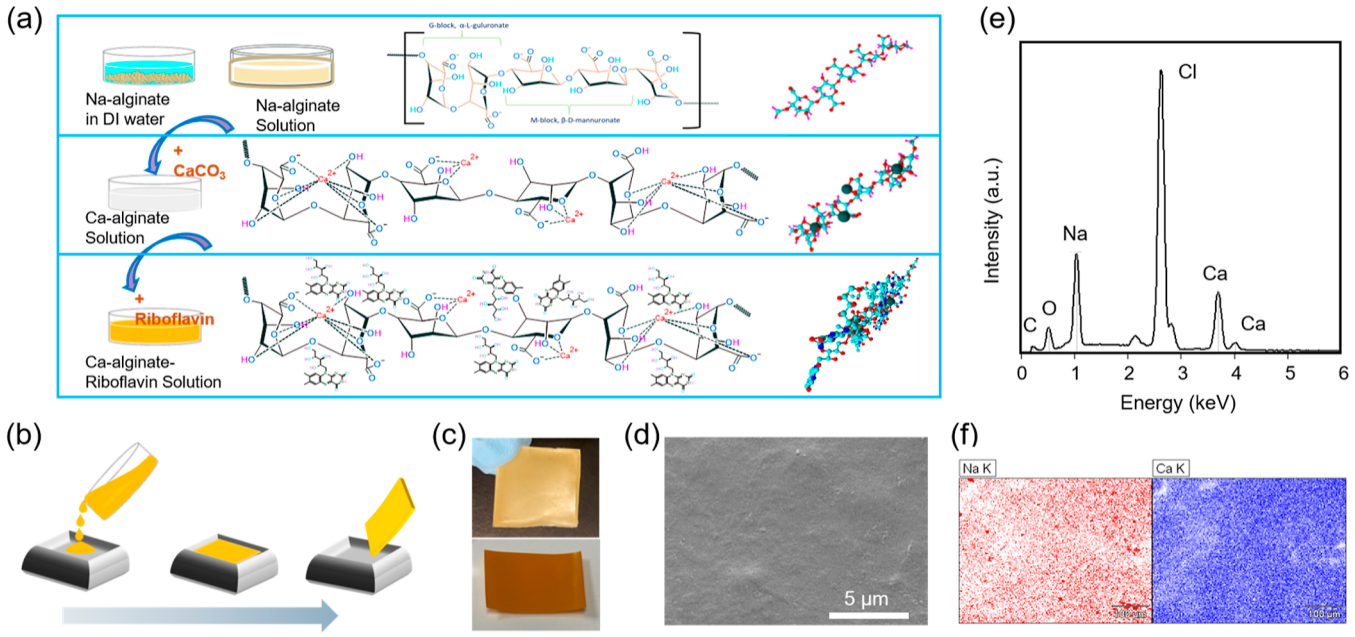

Figure 1. Ca-AR film preparation: (a) schematic illustrations of CA-AR film preparation, including the chemical structure of sodium (Na) and calcium (Ca) alginates and calcium alginate riboflavin as well as their corresponding 3D molecular presentations. (b) Schematic illustrations of Ca-AR film casting. (c) Optical images of prepared films of calcium alginate without riboflavin (top) and Ca-AR (bottom). (d) SEM image of Ca-AR film. (e) EDS spectrum of Ca-AR film. (f) EDS elemental mapping images of Na and Ca.

degradation rate of device components, particularly in pH-dependent oxidative solution-triggering processes.[18,19] Also, the instant disintegration of water-soluble components in aqueous solutions significantly restricts the versatility of transient electronics, which becomes pronounced in situations where precisely controlled transient characteristics are demanded.[20] Furthermore, the functionalities of these solution-degradable substrates in the conventional approaches are limited to introducing the transient characteristics only, without offering any additional values to device performances. Other stimuli, such as heat- and/or light-triggered transient electronics, have been studied as alternatives to the solution-driven transient approaches.[21] These studies include incorporating photoacid generators into metastable polymers[22,23] as well as employing light-responsive hydrogels capable of gel-to-solution transitions.[24] However, the transient characteristics of these photoacid compounds and their photodegradation byproducts have been limitedly applied to biomedical devices only.[25,26]

Herein, we report a novel approach to introduce controlled transient characteristics into wafer-scale 2D MoS_2 devices by employing light-sensitive natural biopolymers as their active device components with additional functionalities. Specifically, we explore riboflavin-incorporated calcium alginate (Ca-AR) films as the media to trigger the transient characteristics and employ them as solid-state electrolyte gates for 2D MoS_2-based field-effect transistors (FETs). The Ca-AR films-incorporated 2D MoS_2 devices exhibit excellent transition characteristics of spontaneous disintegration upon ultraviolet (UV)-to-visible light irradiation in a well-controlled manner. Furthermore, they display noticeable FET gate responses enabled and modulated by the mobile Ca^{2+} ions within the Ca-AR film electrolyte gates, which are also verified by the triboelectric characteristics of the gates. The operation principle for the Ca-AR films-modulated 2D MoS_2 FETs is discussed in the context of the electric double layer (EDL) gating.[27,28]

RESULTS AND DISCUSSION

In pursuing the natural biopolymer of Ca-AR as the medium to introduce the afore-discussed multifunctional transient characteristics, we extensively consider its material properties suitable for transient electronics, i.e., intrinsic biocompatibility, photodegradability owing to its constituent riboflavin, as well as ability to donate mobile ions to create EDLs with a redistributed charge density, all of which have been difficult to accomplish in single solution-based electrolyte materials.[29−31] Sodium alginates, linear polysaccharide salts of alginic acid, are unbranched copolymers of equatorial β-D-mannuronate (M block), and axial α-L-guluronate (G block) possess an inherent affinity to cross-link with polyvalent metal ions.[32] The stoichiometric ratio of ions, such as Ca^{2+} and $COOH^-$ ions, determines the extent of gelation, solubility, conductivity, and mechanical stiffness of calcium alginate hydrogels, films, capsules, and fibers.[33−35] While calcium alginate-based materials have been extensively used in biomedical applications for decades, their integration into electronic and/or optoelectronic devices recently drew attention,[36,37] mainly due to their intrinsic dielectric properties as passive device components.[38] Following the preparation of calcium alginate in a thin film form, isoalloxazine riboflavin 7,8-dimethyl-10(1′-D-ribityl), an essential nutrient in animal and plant metabolism[39] is incorporated into the film. Its specific role is to promote the targeted light-triggered transient characteristics, as it is a natural photosensitizer capable of generating highly reactive oxygen species (ROS) upon exposure to UV−visible light.[40] Figure 1a delineates an overview for preparing Ca-AR films, featuring the chemical structures of Na-alginate, Ca-alginate, and Ca-alginate riboflavin, accompanied by corresponding 3D molecular representations. Details for the step-by-step preparation procedures are described in the Experimental Methods section. In preparing for the films, we employed a "dry-cast gelation" method over the conventionally adopted lyophilization process,[41] as it is more suitable for achieving

https://doi.org/10.1021/acsami.4c09275
ACS Appl. Mater. Interfaces 2024, 16, 39673−39682

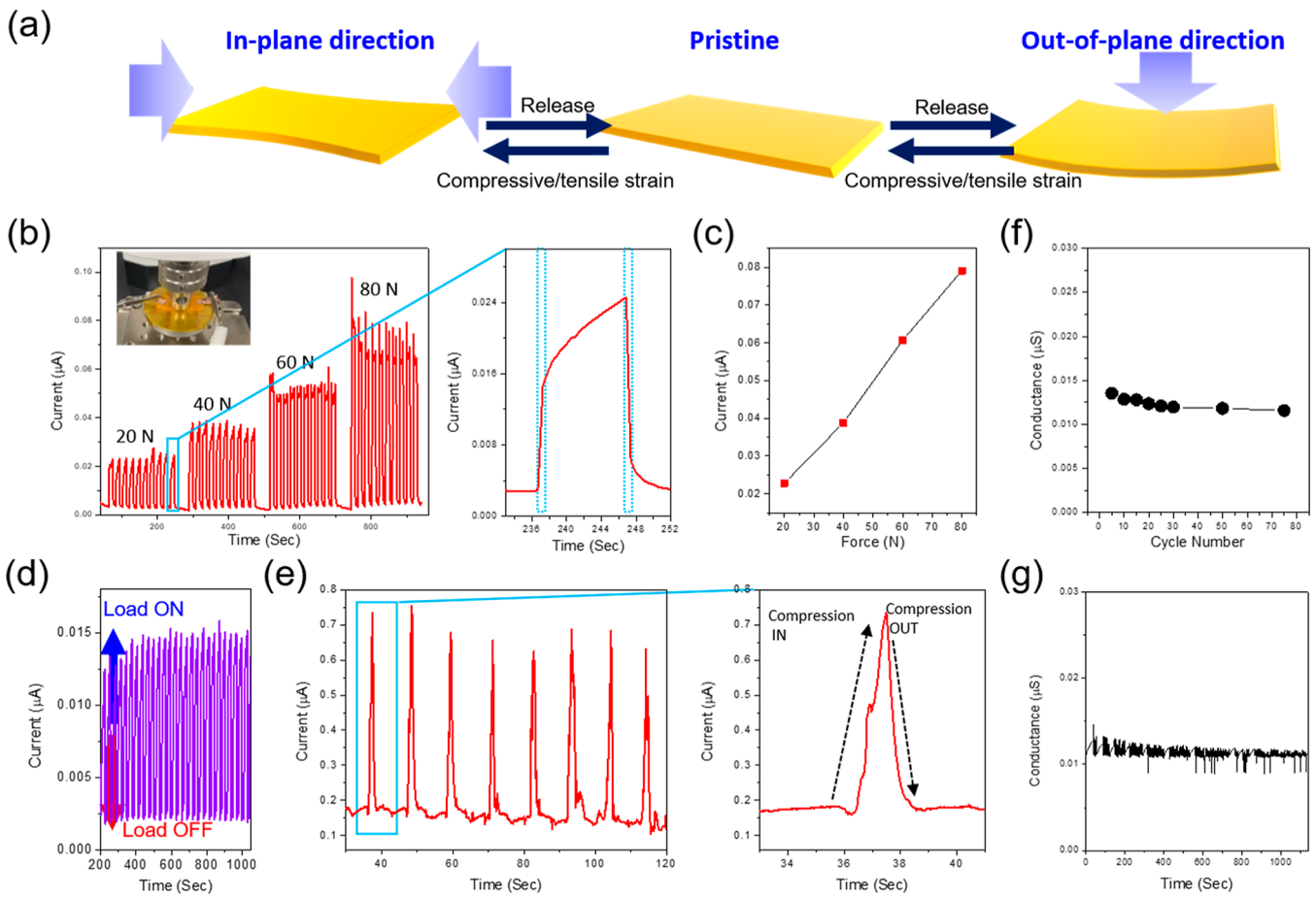

Figure 2. Triboelectric characterization of Ca-AR films. (a) Schematic illustration of in-plane vs out-of-plane strain application. (b) Temporal response of current under out-of-plane force application. (c) Relationship of current vs force. (d) Endurance of current response under prolonged force applications. (e) Temporal response of current under in-plane force application. (f) Relationship of triboelectric conductance vs load application cycle number. (g) Endurance of triboelectric conductance over prolonged time.

highly uniform nonporous films, which are better suited as electrolyte gates for FETs. This method meticulously considers various factors such as the duration of $Ca^{2+}/COOH^{-}$ cross-linking and the entrapment of riboflavin molecules within the calcium alginate matrix toward better minimizing the film porosity and controlling the riboflavin release,[42] as detailed in the Experimental Methods section. Figure 1b illustrates the dry cast gelation method, and Figure 1c presents optical microscopy images of resulting samples at each preparation stage, i.e., as-prepared calcium alginate (top) and calcium alginate containing riboflavin (bottom) films, where the color change results from the incorporation of riboflavin into the calcium alginate matrix. Figure 1d displays a scanning electron microscopy (SEM) image of the prepared Ca-AR film shown in Figure 1c bottom, revealing a highly uniform morphology with minimum porosity. Energy-dispersive X-ray spectroscopy (EDS) characterization was performed on the same sample to identify and quantify its constituent elements. Figure 1e presents a representative EDS spectrum, confirming the presence of multiple elements introduced during the sample preparation procedures in Figure 1a. Figure 1f shows EDS mapping images corresponding to Figure 1e, which clearly reveal that calcium (Ca: left) and sodium (Na: right) elements are uniformly distributed over a large area (>several μm^2), confirming the structural and chemical homogeneity of the film.

Following the material preparation and its associated characterization efforts, we studied the electrical properties of Ca-AR films to gain insights into their suitability as electrolyte gates for FETs. We particularly focus on unveiling their triboelectric characteristics, which are generally driven by the coupling effects of tribo-electrification and electrostatic induction[43,44] in conductive materials containing mobile charges and/or ions—i.e., presumably Ca^{2+} and Na^{+} in our case. For the triboelectricity measurement, the film is subjected to systematically applied combinations of tensile and comprehensive strains in both in-plane and out-of-plane orientations. Figure 2a illustrates that in-plane (left) and out-of-plane (right) strains are periodically applied/released in the sequence of compressive-to-tensile, obtained from a sample in a pristine state (mid). Figure 2b presents temporal responses of current vs time obtained from a sample under systematically applied load amounts of 20, 40, 60, and 80 N in an out-of-plane direction, measured at a bias voltage of 10 V. The measurement was performed with a motorized tension/compression tester (Mark-10 ESM-303) as shown in Figure 2b inset and was analyzed with MESUR gauge software for controlled out-of-plane force application. The sample exhibits a steady increase in current with a cyclic application of out-of-plane strain, indicative of typical triboelectric characteristics.[45] The enlarged view of a plot of current vs single application/release of 20 N reveals quick (<1 s) response times of the film

https://doi.org/10.1021/acsami.4c09275
ACS Appl. Mater. Interfaces 2024, 16, 39673−39682

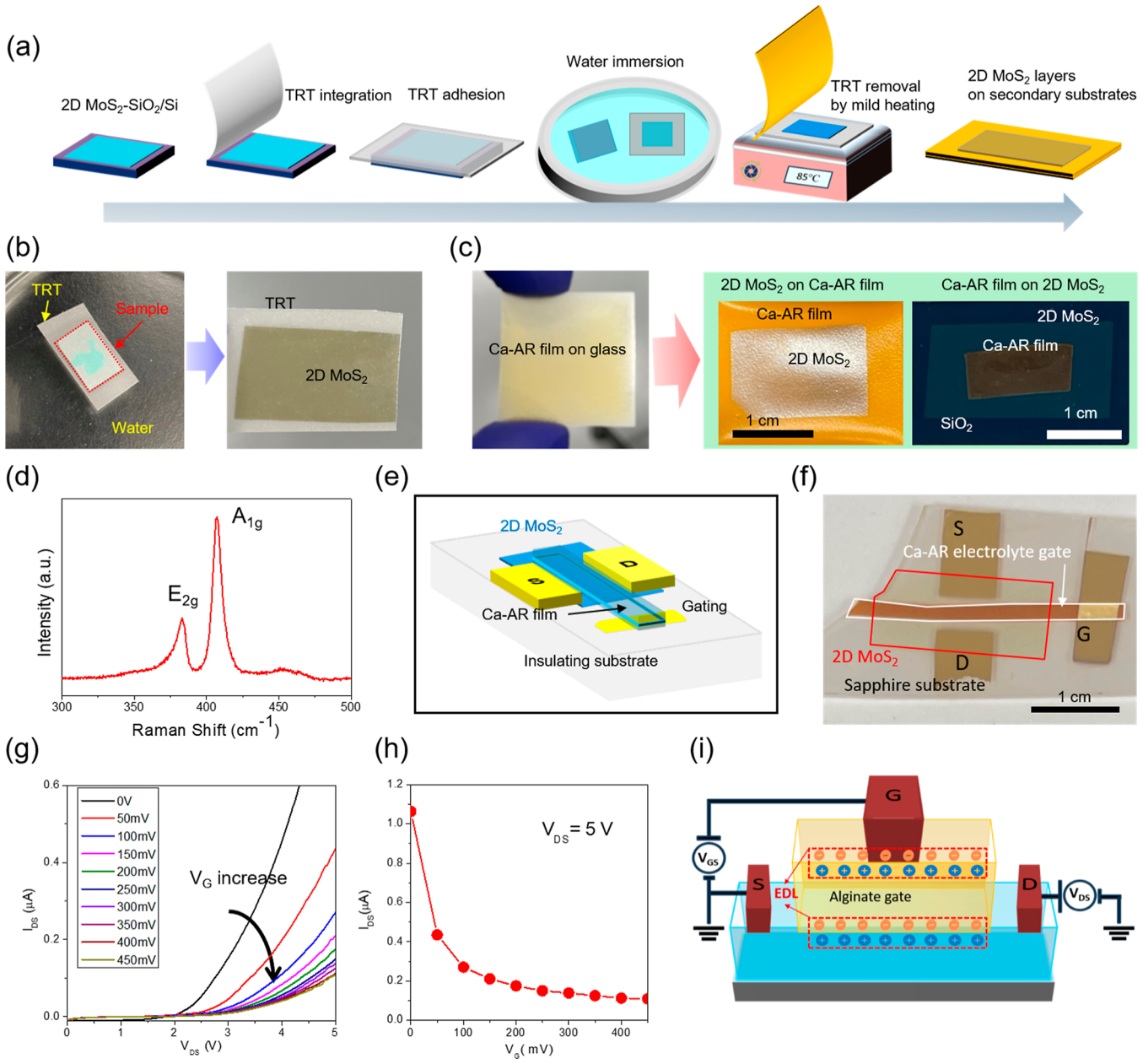

Figure 3. Ca-AR film-incorporated 2D MoS_2 layers-based devices. (a) Schematic illustration of 2D MoS_2 layers delamination and integration. (b) Optical images of water-assisted delamination of TRT/2D MoS_2 layers. (c) Combination of Ca-AR film with delaminated 2D MoS_2 layers. (d) Raman characterization of 2D MoS_2 layers integrated on Ca-AR film. (e) Schematic illustration of Ca-AR gated-2D MoS_2 FET. (f) Optical image of actual FET corresponding to (d). (g) $I_{DS}-V_{DS}$ output characteristics. (h) $I_{DS}-V_G$ transfer characteristics. (i) Schematic illustration of EDL-driven FET gating.

in increasing/decreasing the current. Figure 2c presents a plot of the average maximum current vs corresponding load amount for each measurement period, revealing a nearly linear increase of current with increasing pressure in the tested range of 20–80 N. Figure 2d displays the endurance test of the film in generating triboelectricity for a large number of cyclic application/releases of out-of-plane force up to 1000 s. No degradation in the current generation is observed, which confirms the high mechanical durability and flexibility of the film. In addition to the out-of-plane triboelectricity measurement, the same sample was also subjected to a controlled application/release of in-plane strain by a Zaber motorized linear stage. Figure 2e presents a plot of current vs time obtained from the same sample under a periodic application/release of in-plane strain, where the enlarged view unveils detailed current rise/decay characteristics. Furthermore, we performed reliability tests of the film to verify its long-term reproducibility of triboelectric characteristics as well as its mechanical robustness. Figure 2f shows a plot of average maximum conductance vs cycle numbers obtained under a cyclic application of 50 N out-of-plane load. Figure 2g illustrates a temporal plot of conductance values generated during a prolonged application of the same load for >1200 s, further confirming the excellent electrical durability of the film. These comprehensive characterizations of triboelectric characteristics validate the presence of ions within Ca-AR films, thus substantiating their suitability as solid-state electrolyte gates for FETs, which is presented in the next section. Additionally, we

https://doi.org/10.1021/acsami.4c09275
ACS Appl. Mater. Interfaces 2024, 16, 39673−39682

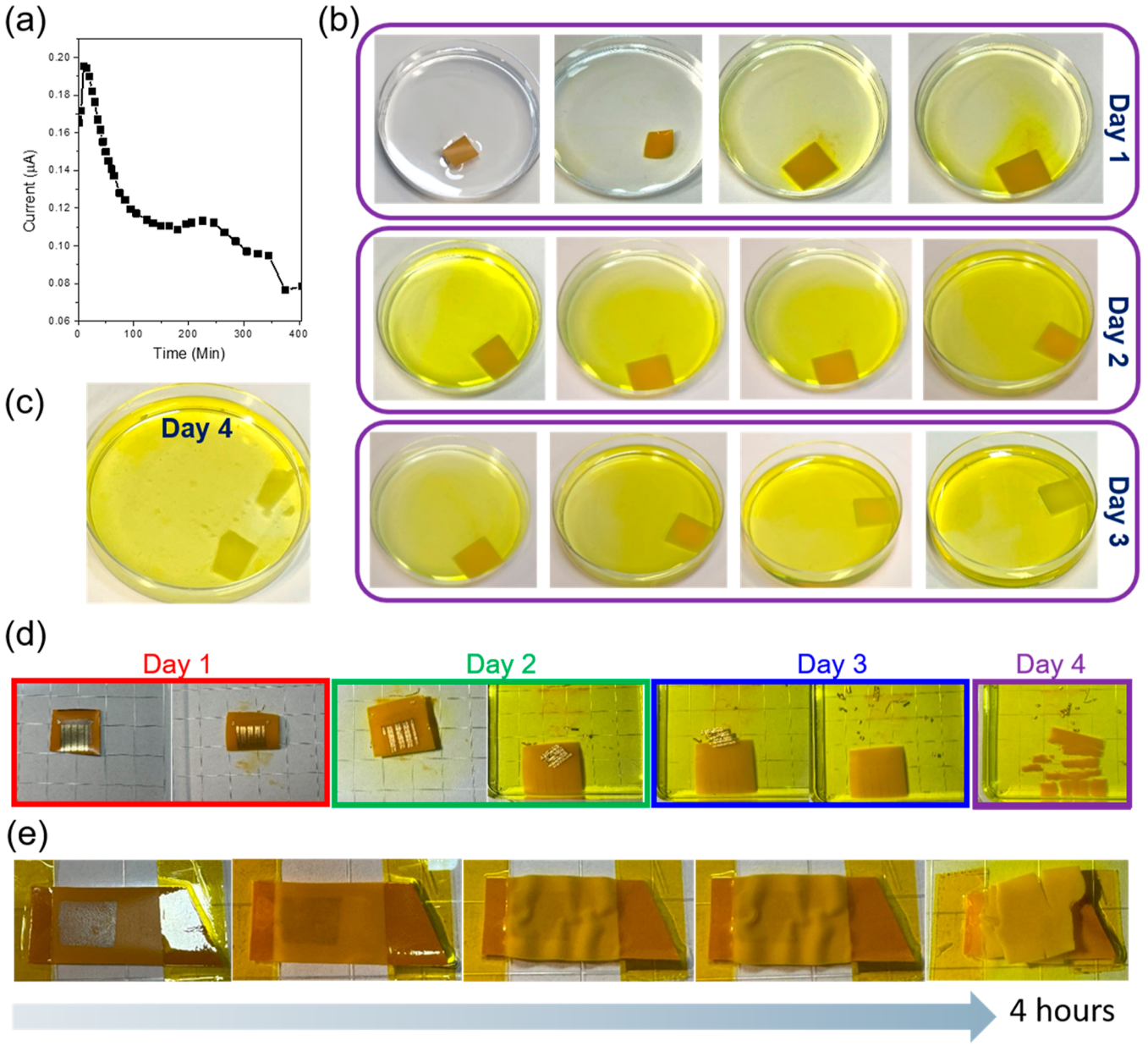

Figure 4. UV and water-driven transient characteristics (a) UV-driven degradation of Ca-AR film manifested by temporal current change. (b) Snap-shot images of dissolving Ca-AR film in water. (c) Complete fragmentation of Ca-AR film. (d) Snap-shot images showing disintegration of Ca-AR incorporated 2D MoS_2 layers-based device. (e) Enhanced degradability of Ca-AR incorporated 2D MoS_2 layers via adjusted cross-linking chemistry.

evaluated the influences of other external stimuli, such as temperature and bending, on the electrical properties of Ca-AR films by manifesting their current−voltage (I−V) characteristics (Supporting Information, Figure S1). Furthermore, we performed AC frequency-dependent capacitance and conductance measurements with a period application/release of out-of-plane strain (Supporting Information, Figure S2), observing frequency-dependent characteristics of ion-conductive polymers.[46,47]

Having confirmed the ionic conductance of Ca-AR films, we then integrated them into 2D MoS_2 layers-based FETs as gate media and explored resulting FET characteristics. The fabrication of 2D MoS_2-based FETs starts with the delamination of as-grown 2D MoS_2 layers off their silicon dioxide/silicon (SiO_2/Si) growth wafers and their subsequent transfer onto secondary insulating substrates (e.g., sapphires). On top of the 2D MoS_2 layers, which function as FET channels, Ca-AR films are selectively integrated as "top" gates to introduce EDL-driven gating into the channels, followed by a patterned deposition of metal electrodes. Figure 3a illustrates step-by-step procedures for delamination of wafer-scale 2D MoS_2 layers grown by the chemical vapor deposition (CVD) method established in our group[48] and their transfer/integration onto secondary substrates. As-grown 2D MoS_2 layers-on-SiO_2/Si are manually attached to a thermal release tape (TRT), and a whole body of TRT/2D MoS_2/SiO_2/Si is immersed in water, which delaminates TRT/2D MoS_2 layers off the SiO_2/Si as previously verified in our studies.[49] Upon integrating the TRT/2D MoS_2 layers onto secondary substrates, mild heating subsequently detaches the TRT.

https://doi.org/10.1021/acsami.4c09275
ACS Appl. Mater. Interfaces 2024, 16, 39673−39682

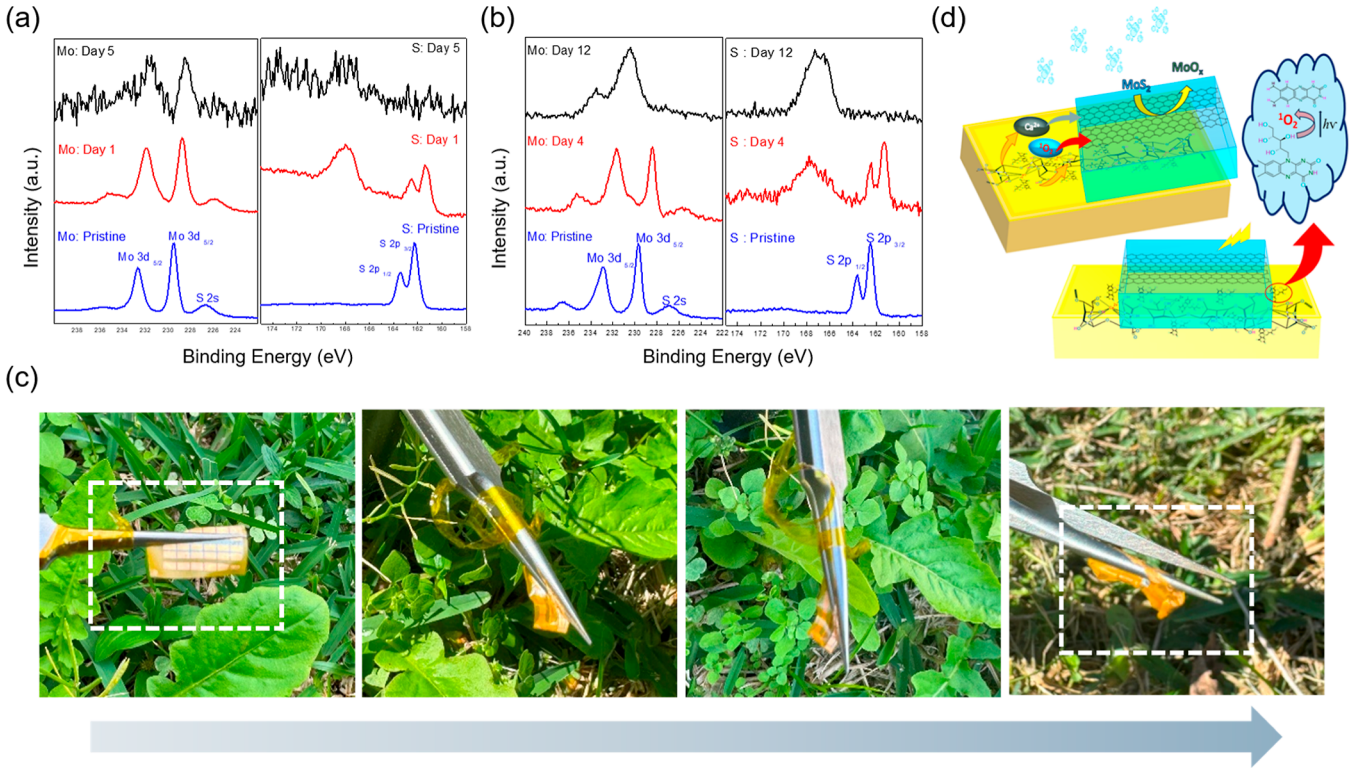

Figure 5. Mechanism study of water and UV−vis driven transient characteristics of Ca-AR incorporated 2D MoS_2 layers. (a,b) XPS characterization of samples treated with (a) aqueous Ca-AR solution and (b) UV−vis light illumination. (c) Spontaneous degradation of Ca-AR incorporated 2D MoS_2 layers-based device in outdoor air. (d) Schematic illustration of molecular interaction of Ca-AR with 2D MoS_2 layers under UV−vis illumination.

Figure 3b shows optical images of sequential delamination procedures for 2D MoS_2 layers, i.e., a sample of TRT/2D MoS_2/SiO_2/Si immersed in water (left) and 2D MoS_2 layers/TRT delaminated from the SiO_2/Si wafer (right). The delaminated 2D MoS_2 layers can be combined with arbitrary substrates and materials, including Ca-AR films, as presented in Figure 3c. The left image in Figure 3c shows an optical image of a Ca-AR film separately prepared on a glass substrate before their integration with 2D MoS_2 layers. The right image in Figure 3c demonstrates two different integration cases: (1) 2D MoS_2 layers on a Ca-AR film and (2) Ca-AR film on 2D MoS_2 layers preintegrated on a secondary SiO_2/Si substrate. This controllable manipulation of Ca-AR/2D MoS_2 heterostructures independent of their integration sequences enables the fabrication of 2D MoS_2-based FETs where Ca-AR film and 2D MoS_2 layers function as top-gate and channels, respectively. Figure 3d presents a Raman spectrum of 2D MoS_2 layers integrated on Ca-AR film, confirming two distinguishable peaks corresponding to the in-plane (E_{2g}^1) and out-of-plane (A_{1g}) vibrational modes of 2D MoS_2 layers.[50] Figure 3e displays a schematic illustration of a 2D MoS_2-based FET with a Ca-AR film top-gate fabricated sequentially integrating Ca-AR film and 2D MoS_2 layers on top of an insulating sapphire substrate. Figure 3f presents an image of an actual FET where the large-area (>cm^2, red box) 2D MoS_2 layers-based channel is interfaced with the Ca-AR film (white box)-based gate (G), which introduces EDL-enabled electrolyte gating into it. The gate-modulated current response across source (S) and drain (D) electrodes is measured with varying gate voltage (V_G). Figure 3g exhibits the FET output characteristics of source current (I_{DS}) vs drain-source voltage (V_{DS}) corresponding to Figure 3f, obtained with varying V_g of 0−450 mV with a step of 50 mV. I_{DS} decreases with increasing V_G, indicating a p-type gate response of the Ca-AR electrolyte-gated 2D MoS_2 FET. Figure 3h presents the corresponding I_{DS}−V_G transfer curve obtained at V_{DS} = 5 V, which further confirms the pronounced p-type gate response manifested by decreasing corresponding I_{DS} with increasing V_G, consistent with our previous studies.[51] The observations strongly support that the Ca-AR film top gate can efficiently gate the 2D MoS_2 layers-based channel owing to its ion-conductive electrolyte nature. The gating mechanism is attributed to the formation of EDL at the interface of 2D MoS_2 layers (channel)/Ca-AR film (gate), as illustrated in Figure 3i. As proposed, when a negative V_G is applied to the top Au electrode, an attraction of cations (Ca^{2+}/Na^+) within the Ca-AR electrolyte near the electrode leads to a repulsion of anions ($COOH^-$/OH^-) toward the interface of Ca-AR/2D MoS_2 layers forming EDL, which results in an accumulation of positivity within the 2D MoS_2 layers.[52] Accordingly, the hole conductivity of the FET channel increases, which becomes more pronounced with further decreasing V_G (i.e., more negative V_G).[53,54] This concept of EDL-driven gate modulation adopting electrolyte media is well established in the literature, and our proposed gating mechanism model in Figure 3i well agrees with previous studies.[55,56] We also tested Ca-AR/2D MoS_2 layers-based FETs with slightly modified gate configurations and observed qualitatively similar FET gate responses (Supporting Information, Figure S3).

Following the successful proof-of-concept demonstration of operating 2D MoS_2 FETs via the EDL mechanism, we then explored their transient characteristics enabled by the Ca-AR films integrated into them. We first focused on unveiling the

https://doi.org/10.1021/acsami.4c09275
ACS Appl. Mater. Interfaces 2024, 16, 39673−39682

intrinsic transient characteristics of stand-alone Ca-AR films before their device integration under UV illumination. Figure 4a presents a temporal plot of current values measured with a stand-alone Ca-AR film sample under continuous exposure to UV-C (253.7 nm wavelength).[57] The plot reveals a gradual decrease in current with time, reflecting a steady degradation of photosensitizing riboflavin within the Ca-AR film. In addition to the light-triggered transient characteristics, we also investigated a water-driven degradation of the Ca-AR film exposed to deionized (DI) water. This approach was aimed to take advantage of the presence of Na^+, a water-soluble monovalent salt of alginic acid, within the Ca-AR film introduced during its preparation state (Figure 1a). The water-driven degradability of the Ca-AR film is controllable by considering the water solubility of polyvalent alginic acid salt, i.e., Ca-alginate, which depends on the degrees of ion substitution between Na^+ and Ca^{2+} as well as cross-linking between Ca^+ and $COOH^-$ ions.[58,59] Figure 4b shows snapshot images of the water-driven degradation of the Ca-AR film, which gradually turns white during the course of 3 days, while the orange color represents a release of riboflavin. On day 4, it is noted that the film becomes completely fragmented, accompanying the color change, as shown in Figure 4c. Upon confirming the intrinsic water degradability of Ca-AR films, we tested the water-driven transient characteristics of 2D MoS_2 layers-based FETs with Au electrodes and Ca-AR films integrated. Figure 4d displays snapshot images of a representative sample of a 2D MoS_2 layers-based device undergoing gradual disintegration within DI water, activated by its constituent Ca-AR film. The transition characteristics are observed to be similar to those with stand-alone Ca-AR films in Figure 4b,c. In a way to demonstrate the controllability of the degradation kinetics of Ca-AR films, we also prepared Na^+-rich films with minimal Ca^{2+} cross-linking (EDS spectrum in Supporting Information, Figure S4) followed by integrating 2D MoS_2 layers. Figure 4e presents the transient characteristics of the corresponding sample, which exhibits a much faster degradability, showing its significant fragmentation within 4 h compared to Figure 4b−d, consistent with previous studies.[60]

In order to clarify the mechanism for the Ca-AR films-driven degradation of 2D MoS_2 layers, we performed X-ray photoelectron spectroscopy (XPS) characterizations of Ca-AR/2D MoS_2 layer samples under UV-visible or water exposure, focusing on identifying their oxidation states. Figure 5a presents the Mo (left column) and S (right column) core-level binding energy XPS spectra of 2D MoS_2 layers in their pristine state vs sequentially treated with Ca-AR aqueous solution for up to 5 days. Previous studies on the photodegradation of riboflavin present in Ca-alginate solutions suggest the presence of various factors influencing its degradation efficacy, such as pH, ratios of cations (Ca^{2+}/Na^+) and anions ($COOH^-$/CO_3^{2-}/Cl^-), as well as illumination intensity.[61] Additionally, other studies as well as our own investigations, report that the oxidation and dissolution of 2D MoS_2 layers can be significantly promoted with a presence of ions such as Na^+.,[62,63] In Figure 5a, the sample in its pristine state (blue) exhibits XPS peaks corresponding to Mo $3d_{5/2}$ (229.4 eV), Mo $3d_{3/2}$ (232.6 eV), and S 2s (226. eV)—shown on the left column, and the XPS spectra for the S 2p core level obtained at $2p_{3/2}$ (162.3 eV) and S $2p_{1/2}$ (163.5 eV) indicate a presence of pristine sulfide (S^{2-})—shown on the right column.[64] Once the sample is treated with the Ca-AR solution for 1 day, it starts to exhibit satellite peaks on the Mo core level XPS spectra (left column) at 235.2 eV on day 1 (red), implying a molecular interaction of MoS_2 with ions in the solution. Such phenomena are commonly observed with 2D MoS_2 layers interacting with conducting polymers, as verified in previous studies on 2D MoS_2 layers-based hydrogen evolution reaction.[65] Moreover, the presence of Mo $3d_{3/2}$ (232.3 eV) and Mo $3d_{5/2}$ (229.1 eV) coupled with the disappearance of the S 2s peak signify a change in the oxidation state of Mo from +4 to +5. On the S 2p core level spectra (right column), an additional satellite peak appears at 168.0 eV on day 1 (red), indicating a formation of a sulfide bond (S^{2-}) with the alginate polymer.[66] However, once the sample undergoes a significantly prolonged treatment for 5 days, it becomes impossible to clearly discern XPS characteristic peaks, suggesting a dissolution of reaction products within the solution. We also performed XPS characterizations of Ca-AR incorporated 2D MoS_2 layers sequentially exposed to UV−vis illumination. Figure 5b presents the Mo 3d (left column) and S 2s (right column) core levels XPS spectra of Ca-AR incorporated 2D MoS_2 layers before and after the light illumination. The sample in its pristine state (blue) exhibits well-defined XPS peaks corresponding to Mo $3d_{5/2}$ (229.5 eV), Mo $3d_{3/2}$ (232.6 eV), and S 2s (226.6 eV) on the left column as well as $2p_{3/2}$ (162.3 eV) and S $2p_{1/2}$ (163.5 eV) for the S 2p core level (right column).[64] The sample is subsequently irradiated by a solar simulator (UV−vis spectrum in a range of 350−1100 nm) under ambient room conditions for prolonged periods. Noticeable shifts and disappearances of the original peaks accompanying the appearance of new peaks are observed, which indicates a change in the oxidation states of 2D MoS_2 layers. For instance, on the S 2p core level XPS spectra (right column), a new peak is observed at 167.8 eV on day 4, and the original $2p_{3/2}$ and S $2p_{1/2}$ peaks completely disappear after 12 days of illumination. After a light illumination for 12 days, the Mo 3d core level XPS spectra correspond to Mo $3d_{5/2}$ (230.4 eV) and Mo $3d_{3/2}$ (233.5 eV), indicating the oxidation state of Mo^{4+} shifting to Mo^{6+} and the S 2p core level XPS peak obtained at 167.3 eV implies an S^{2-} bond formation with polymers, in this case, the Ca-AR film.[67] These comprehensive characterizations support that Ca-AR films are highly sensitive to both light and water, triggering the controlled dissociation of 2D MoS_2 layers, which involves an alteration of their molecular oxidation states—e.g., the formation of Mo oxides. Based on this confirmation, we tested the spontaneous degradability of Ca-AR-incorporated 2D MoS2 layers-based devices with Au electrodes by exposing them to open air involving both natural sunlight and humidity. Figure 5c presents snapshot images of a sample device exposed outdoors during the course of 4 days. The initially pristine device (white box in the first image) exhibits a significant structural distortion after 4 days, even without any externally applied stimuli in the natural environment. Lastly, we propose the underlying mechanism for the Ca-AR-driven degradation of 2D MoS_2 layers in the context of their molecular interactions, as presented in Figure 5d. Molecules of alloxazine riboflavin incorporated into calcium alginate composites are known to exhibit a broad span of absorbance spectra, undergoing photodegradation upon exposure to UV−vis light illuminations.[68] Our study mainly focuses on investigating the UV−vis light-induced oxidation of 2D MoS_2 layers, which generates ROS, a byproduct of the photodegraded riboflavin. In a basic medium, the photodegraded riboflavin is known to form various species, such as formylmethylflavin, lumichrome

https://doi.org/10.1021/acsami.4c09275
ACS Appl. Mater. Interfaces 2024, 16, 39673−39682

(LC), and lumiflavin, along with ROS, specifically, singlet oxygen ($^1O_2$)[69,70] For simplicity, the schematic illustration in Figure 5d focuses on a formation of LC (main photodegradation product) and its subsequent generation of $^1O_2$. As depicted, these products released from Ca-AR films coupled with ambient water molecules facilitate the oxidation of 2D MoS_2 layers, promoting the formation of MoO_X, as supported by XPS analysis. The accelerated degradation of Ca-AR via a combined application of light and humidity is attributed to the presence of charged species, such as Na^+, Ca^{2+}, OH^-, and $COOH^-$, which further facilitates the rapid oxidation of 2D MoS_2 layers.

CONCLUSION

This study innovatively incorporates calcium alginate as an active component in a 2D MoS_2 layers-based devices, presenting a viable approach to introduce their controlled transient characteristics. The key to the success of realizing the transient devices is to integrate a riboflavin photosensitizer into them and engineer its cross-linking chemistry associated with constituent mobile ions toward optimized degradability. The suitability of the Ca-AR as the active device component is supported by its strain-driven triboelectric properties, which justify the electrolyte gating operation of 2D MoS_2 FETs. Ca-AR/2D MoS_2 layers-based devices in various forms exhibit the targeted transient characteristics under various external stimuli—i.e., UV−vis light illumination, humidity incorporation, and outdoor exposure to natural sunlight. The fundamental mechanism for the stimuli-triggered dissociation of Ca-AR and its influence on disintegrating 2D MoS_2 layers is discussed in the framework of their molecular interaction and oxidation state changes, also verified by XPS characterizations. This study demonstrates a new venue for heterogeneously integrating natural polymers with 2D atom-thickness semiconductors in the direction of futuristic device concepts.

EXPERIMENTAL METHODS

Calcium Alginate Riboflavin Film Preparation. 5.0 g of sodium alginate (Sigma-Aldrich) is dissolved in 250 mL DI water and stirred with a magnetic stirrer at room temperature overnight to prepare a stock solution. Water-insoluble $CaCO_3$ (Sigma-Aldrich) is used to limit the extent of Ca^{2+} cross-linking with Na-alginate. 100 mL of Na-alginate solution is mixed with 0.25 g of $CaCO_3$ and 0.1 g of riboflavin and stirred with a magnetic stirrer overnight in an amber glass bottle to prevent the photodegradation of riboflavin. 100 mL of Na-alginate solution is mixed with 1.0−2.5 g of water-soluble $CaCl_2$ (Sigma-Aldrich), which is used to increase the Ca^{2+} cross-linking. 0.1 g of riboflavin is added to the solution and is stirred with a magnetic stirrer for 2 h in an amber glass bottle. The uniform solution mixtures are cast on a Petri dish and are subsequently stored in the dark at room temperature for 4 days, which leads to the formation of films through solvent evaporations. Thin films of calcium alginate riboflavin adopted for FET gates are prepared by solution casting on glass slides using a spin coater at 1500−2000 rpm.

CVD Growth of Centimeter-Scale 2D MoS_2 Layers. One nanometer thickness Mo films are deposited on sapphire and SiO_2/Si wafers thoroughly cleaned by acetone, isopropyl alcohol, and DI water, using an e-beam evaporator (Thermionics VE-100). The Mo-deposited wafers are placed within a quartz tube at the center zone of a CVD furnace (Lindberg/Blue M Mini-Mite) along with alumina boats holding S precursor placed at the furnace upstream side. Once the base pressure of the quartz tube reaches ∼10 mTorr, Ar gas is flushed into it to remove any residuals. The CVD furnace is set to gradually ramp up to reach the growth temperature of 850 °C, and the S powder is set to vaporize at ∼200 °C. The reaction is maintained for 60 min under a constant supply of Ar gas at a 100 sccm flow rate. After the reaction, the furnace is naturally cooled down to room temperature.

Characterizations with Raman, XPS, and SEM. A 532 nm excitation laser at room temperature is used for Raman characterization on Horiba LabRAM HR Evolution instrument. XPS characterizations are conducted with ESCALAB 250 (Thermo Fisher Scientific) in an ultrahigh vacuum (10^{-9} mbar). SEM and EDS characterizations are performed using Zeiss ULTRA-55 FEG scanning electron microscope.

Electrical Measurements. Semiconductor parameter analyzers Keysight B1500A and HP 4156 A, connected with a home-built probe station, are used for all electrical measurements, including triboelectricity and FET. Triboelectricity measurements are also performed with a motorized tension/compression tester (Mark-10 ESM-303) operated by MESUR gauge software.

ASSOCIATED CONTENT

Supporting Information

The Supporting Information is available free of charge at https://pubs.acs.org/doi/10.1021/acsami.4c09275.

Temperature and bending-dependent $I-V$ characteristics (S1), AC frequency-dependent measurements of capacitance and conductance with a period application/release of out-of-plane strain (S2), Ca-AR/2D MoS_2 layers-based FETs with slightly modified gate configurations and corresponding $I_{DS}-V_G$ transfer curves (S3), and EDS spectrum of Na^+-rich alginate film (S4) (PDF)

AUTHOR INFORMATION

Corresponding Author

Yeonwoong Jung − *Department of Materials Science and Engineering, University of Central Florida, Orlando, Florida 32816, United States; NanoScience Technology Center, University of Central Florida, Orlando, Florida 32826, United States; Department of Electrical and Computer Engineering, University of Central Florida, Orlando, Florida 32816, United States;* orcid.org/0000-0001-6042-5551; Email: yeonwoong.jung@ucf.edu

Authors

Md Golam Kaium − *Department of Materials Science and Engineering, University of Central Florida, Orlando, Florida 32816, United States*

Sang Sub Han − *NanoScience Technology Center, University of Central Florida, Orlando, Florida 32826, United States*

Chung Won Lee − *NanoScience Technology Center, University of Central Florida, Orlando, Florida 32826, United States*

Complete contact information is available at: https://pubs.acs.org/10.1021/acsami.4c09275

Author Contributions

M.G.K. conceived the project idea under the guidance and direction of Y.J. M.G.K. prepared the samples and conducted the triboelectric characterizations. M.G.K. performed the FET device fabrication and measurement assisted by S.S.H. C.W.L. performed the Raman characterization. M.G.K. performed the SEM and EDS characterization. M.G.K. conducted the dissolution and degradation experiments and XPS characterization. M.G.K. and Y.J. wrote the manuscript with inputs from all authors.

Notes

The authors declare no competing financial interest.

https://doi.org/10.1021/acsami.4c09275
ACS Appl. Mater. Interfaces 2024, 16, 39673−39682

■ ACKNOWLEDGMENTS

Y.J. acknowledges financial support from the US National Science Foundation (CAREER: 2142310). S.S.H. acknowledges financial support from the Preeminent Postdoctoral Program (P3) at UCF.

■ REFERENCES

(1) Fu, K. K.; Wang, Z.; Dai, J.; Carter, M.; Hu, L. Transient Electronics: Materials and Devices. *Chem. Mater.* **2016**, *28* (11), 3527−3539.
(2) Heacock, M.; Kelly, C. B.; Asante, K. A.; Birnbaum, L. S.; Bergman, Å. L.; Bruné, M.-N.; Buka, I.; Carpenter, D. O.; Chen, A.; Huo, X.; et al. E-Waste and Harm to Vulnerable Populations: A Growing Global Problem. *Environ. Health Perspect.* **2016**, *124* (5), 550−555.
(3) Hwang, S.-W.; Tao, H.; Kim, D.-H.; Cheng, H.; Song, J.-K.; Rill, E.; Brenckle, M. A.; Panilaitis, B.; Won, S. M.; Kim, Y.-S.; et al. A Physically Transient Form of Silicon Electronics. *Science* **2012**, *337* (6102), 1640−1644.
(4) Nazari, L.; Xu, C.; Ray, M. B. Recovery of Metals from Electronic Waste. In *Advanced and Emerging Technologies for Resource Recovery from Wastes*; Nazari, L., Xu, C., Ray, M. B., Eds.; Springer Singapore, 2021; pp 127−156.
(5) Ahirwar, R.; Tripathi, A. K. E-waste Management: A Review of Recycling Process, Environmental and Occupational Health Hazards, and Potential Solutions. *Environ. Nanotechnol., Monit. Manage.* **2021**, *15*, 100409.
(6) Feig, V. R.; Tran, H.; Bao, Z. Biodegradable Polymeric Materials in Degradable Electronic Devices. *ACS Cent. Sci.* **2018**, *4* (3), 337−348.
(7) Li, W.; Liu, Q.; Zhang, Y.; Li, C. a.; He, Z.; Choy, W. C. H.; Low, P. J.; Sonar, P.; Kyaw, A. K. K. Biodegradable Materials and Green Processing for Green Electronics. *Adv. Mater.* **2020**, *32* (33), 2001591.
(8) Dutta, A.; Cheng, H. Pathway of Transient Electronics Towards Connected Biomedical Applications. *Nanoscale* **2023**, *15* (9), 4236−4249.
(9) Fanelli, A.; Ghezzi, D. Transient Electronics: New Opportunities for Implantable Neurotechnology. *Curr. Opin. Biotechnol.* **2021**, *72*, 22−28.
(10) Pandey, S. S.; Banerjee, N.; Xie, Y.; Mastrangelo, C. H. Self-Destructing Secured Microchips by On-Chip Triggered Energetic and Corrosive Attacks for Transient Electronics. *Adv. Mater. Technol.* **2018**, *3* (7), 1800044.
(11) Shin, J.-W.; Chan Choe, J.; Lee, J. H.; Han, W. B.; Jang, T.-M.; Ko, G.-J.; Yang, S. M.; Kim, Y.-G.; Joo, J.; Lim, B. H.; et al. Biologically Safe, Degradable Self-Destruction System for On-Demand, Programmable Transient Electronics. *ACS Nano* **2021**, *15* (12), 19310−19320.
(12) Kang, S.-K.; Hwang, S.-W.; Cheng, H.; Yu, S.; Kim, B. H.; Kim, J.-H.; Huang, Y.; Rogers, J. A. Dissolution Behaviors and Applications of Silicon Oxides and Nitrides in Transient Electronics. *Adv. Funct. Mater.* **2014**, *24* (28), 4427−4434.
(13) Wang, S.; Dang, B.; Sun, J.; Zhao, M.; Yang, M.; Ma, X.; Wang, H.; Hao, Y. Physically Transient W/ZnO/MgO/W Schottky Diode for Rectifying and Artificial Synapse. *IEEE Electron Device Lett.* **2020**, *41* (6), 844−847.
(14) Xue, Q.; Hang, T.; Gong, Z.; Chen, L.; Liang, J.; Sun, Y.; Lu, D.; Zhang, X.; Chen, C.-C.; Li, M. Transient and Biocompatible Resistive Switching Memory Based on Electrochemically-Deposited Zinc Oxide. *Adv. Electron. Mater.* **2021**, *7* (12), 2100322.
(15) Liu, K.; Wu, J. Mechanical Properties of Two-dimensional Materials and Heterostructures. *J. Mater. Res.* **2016**, *31* (7), 832−844.
(16) Yoo, C.; Ko, T.-J.; Kaium, M. G.; Martinez, R.; Islam, M. M.; Li, H.; Kim, J. H.; Cao, J.; Acharya, M.; Roy, T.; et al. A Minireview on 2D Materials-enabled Optoelectronic Artificial Synaptic Devices. *APL Mater.* **2022**, *10* (7), 070702.
(17) Pucher, T.; Bastante, P.; Parenti, F.; Xie, Y.; Dimaggio, E.; Fiori, G.; Castellanos-Gomez, A. Biodegradable Albumen Dielectrics for High-mobility MoS_2 Phototransistors. *npj 2D Mater. Appl.* **2023**, *7* (1), 73.
(18) Lei, D.; Wu, Z.; Zhang, Y.; Zhang, Y.; Zhang, J.; Xue, J.; Peng, X.; Wang, Y. New Insight Into the Inevitable Oxidation-Dissolution Behavior of MoS_2 at Humid Environments: Unexpected Persistent Generation of Hydroxyl Radicals. *Sep. Purif. Technol.* **2024**, *332*, 125800.
(19) Wang, Z.; von dem Bussche, A.; Qiu, Y.; Valentin, T. M.; Gion, K.; Kane, A. B.; Hurt, R. H. Chemical Dissolution Pathways of MoS_2 Nanosheets in Biological and Environmental Media. *Environ. Sci. Technol.* **2016**, *50* (13), 7208−7217.
(20) Chen, Y.; Lu, H.; Xiu, F.; Sun, T.; Ding, Y.; Liu, J.; Huang, W. Transient Light Emitting Devices Based on Soluble Polymer Composites. *Sci. Rep.* **2018**, *8* (1), 6408.
(21) Lee, G.; Choi, Y. S.; Yoon, H.-J.; Rogers, J. A. Advances in Physicochemically Stimuli-responsive Materials for On-demand Transient Electronic Systems. *Matter* **2020**, *3* (4), 1031−1052.
(22) Kikkawa, Y.; Tanaka, S.; Norikane, Y. Photo-triggered Enzymatic Degradation of Biodegradable Polymers. *RSC Adv.* **2017**, *7* (88), 55720−55724.
(23) Zhong, S.; Ji, X.; Song, L.; Zhang, Y.; Zhao, R. Enabling Transient Electronics with Degradation on Demand via Light-Responsive Encapsulation of a Hydrogel-Oxide Bilayer. *ACS Appl. Mater. Interfaces* **2018**, *10* (42), 36171−36176.
(24) Hernandez, H. L.; Kang, S.-K.; Lee, O. P.; Hwang, S.-W.; Kaitz, J. A.; Inci, B.; Park, C. W.; Chung, S.; Sottos, N. R.; Moore, J. S.; et al. Triggered Transience of Metastable Poly(phthalaldehyde) for Transient Electronics. *Adv. Mater.* **2014**, *26* (45), 7637−7642.
(25) Brown, M. A.; De Vito, S. C. Predicting Azo Dye Toxicity. *Crit. Rev. Environ. Sci. Technol.* **1993**, *23* (3), 249−324.
(26) Walker, R. The Metabolism of Azo Compounds: A Review of the Literature. *Food Cosmet. Toxicol.* **1970**, *8* (6), 659−676.
(27) Wu, B.; Wang, X.; Tang, H.; Jiang, W.; Chen, Y.; Wang, Z.; Cui, Z.; Lin, T.; Shen, H.; Hu, W.; et al. Multifunctional MoS_2 Transistors with Electrolyte Gel Gating. *Small* **2020**, *16* (22), 2000420.
(28) Zhong, C.; Deng, Y.; Roudsari, A. F.; Kapetanovic, A.; Anantram, M. P.; Rolandi, M. A Polysaccharide Bioprotonic Field-effect Transistor. *Nat. Commun.* **2011**, *2* (1), 476.
(29) Fan, Q.; Wang, L.; Xu, D.; Duo, Y.; Gao, J.; Zhang, L.; Wang, X.; Chen, X.; Li, J.; Zhang, H. Solution-gated Transistors of Two-dimensional Materials for Chemical and Biological Sensors: Status and Challenges. *Nanoscale* **2020**, *12* (21), 11364−11394.
(30) Rühl, S.; Heyl, M.; Gärisch, F.; Blumstengel, S.; Ligorio, G.; List-Kratochvil, E. J. W. Benchmarking Electrolyte-Gated Monolayer MoS_2 Field-Effect Transistors in Aqueous Environments. *Phys. Status Solidi RRL* **2021**, *15* (9), 2100147.
(31) Zhao, Y.; Bertolazzi, S.; Maglione, M. S.; Rovira, C.; Mas-Torrent, M.; Samorì, P. Molecular Approach to Electrochemically Switchable Monolayer MoS_2 Transistors. *Adv. Mater.* **2020**, *32* (19), 2000740.
(32) Lee, K. Y.; Mooney, D. J. Alginate: Properties and Biomedical Applications. *Prog. Polym. Sci.* **2012**, *37* (1), 106−126.
(33) Costa, M. J.; Marques, A. M.; Pastrana, L. M.; Teixeira, J. A.; Sillankorva, S. M.; Cerqueira, M. A. Physicochemical Properties of Alginate-based Films: Effect of Ionic Crosslinking and Mannuronic and Guluronic Acid Ratio. *Food Hydrocolloids* **2018**, *81*, 442−448.
(34) Park, S. H.; Lee, S. J. Advanced Molecular Interaction in Cu^{2+}-alginate Beads with High M/G Ratio for the Intercalation of Li^+ and Mg^{2+} Ions. *J. Mol. Struct.* **2019**, *1187*, 172−178.
(35) Russo, R.; Malinconico, M.; Santagata, G. Effect of Cross-Linking with Calcium Ions on the Physical Properties of Alginate Films. *Biomacromolecules* **2007**, *8* (10), 3193−3197.
(36) Ahmad Raus, R.; Wan Nawawi, W. M. F.; Nasaruddin, R. R. Alginate and Alginate Composites for Biomedical Applications. *Asian J. Pharm. Sci.* **2021**, *16* (3), 280−306.
(37) Attia, M. S.; Mohamed, A. A.; El-Saady, M. M.; Abou-Omar, M. N.; Afify, H. G.; Amin, T. A.; Hosny, A. H.; Youssef, A. O.; Mohy-

https://doi.org/10.1021/acsami.4c09275
ACS Appl. Mater. Interfaces 2024, 16, 39673−39682

Eldin, M. S. A New Method for Early Diagnosis of Liver Cancer Using A Biosensor Embedded in An Alginate Polymer Thin Film. *J. Mater. Chem. C* **2022**, *10* (16), 6464−6472.
(38) Li, J.; Wu, Y.; He, J.; Huang, Y. A New Insight to the Effect of Calcium Concentration on Gelation Process and Physical Properties of Alginate Films. *J. Mater. Sci.* **2016**, *51* (12), 5791−5801.
(39) Saedisomeolia, A.; Ashoori, M. Chapter Two—Riboflavin in Human Health: A Review of Current Evidences. In *Advances in Food and Nutrition Research*; Eskin, N. A. M., Ed.; Academic Press, 2018; Vol. *83*, pp 57−81.
(40) Huang, R.; Choe, E.; Min, D. B. Kinetics for Singlet Oxygen Formation by Riboflavin Photosensitization and the Reaction between Riboflavin and Singlet Oxygen. *J. Food Sci.* **2004**, *69* (9), C726−C732.
(41) Arzate-Vázquez, I.; Chanona-Pérez, J. J.; Calderón-Domínguez, G.; Terres-Rojas, E.; Garibay-Febles, V.; Martínez-Rivas, A.; Gutiérrez-López, G. F. Microstructural Characterization of Chitosan and Alginate Films by Microscopy Techniques and Texture Image Analysis. *Carbohydr. Polym.* **2012**, *87* (1), 289−299.
(42) Bajpai, S. K.; Dubey, S. Dynamic Release of Vitamin B2 from Floating Barium Alginate Beads for Gastric Delivery. *J. Macromol. Sci., Part A: Pure Appl.Chem.* **2007**, *44* (9), 1005−1011.
(43) Wang, Y.; Yang, Y.; Wang, Z. L. Triboelectric Nanogenerators as Flexible Power Sources. *npj Flexible Electron.* **2017**, *1* (1), 10.
(44) Wu, C.; Wang, A. C.; Ding, W.; Guo, H.; Wang, Z. L. Triboelectric Nanogenerator: A Foundation of the Energy for the New Era. *Adv. Energy Mater.* **2019**, *9* (1), 1802906.
(45) Pang, Y.; Xi, F.; Luo, J.; Liu, G.; Guo, T.; Zhang, C. An alginate film-based degradable triboelectric nanogenerator. *RSC Adv.* **2018**, *8* (12), 6719−6726.
(46) Bekin, S.; Sarmad, S.; Gürkan, K.; Yenici, G.; Keçeli, G.; Gürdağ, G. Dielectric, Thermal, and Swelling Properties of Calcium Ion-crosslinked Sodium Alginate Film. *Polym. Eng. Sci.* **2014**, *54* (6), 1372−1382.
(47) Láng, G.; Bácskai, J.; Inzelt, G. Impedance Analysis of Polymer Film Electrodes. *Electrochim. Acta* **1993**, *38* (6), 773−780.
(48) Islam, M. A.; Kim, J. H.; Ko, T.-J.; Noh, C.; Nehate, S.; Kaium, M. G.; Ko, M.; Fox, D.; Zhai, L.; Cho, C.-H.; et al. Three dimensionally-ordered 2D MoS_2 Vertical Layers Integrated on Flexible Substrates with Stretch-Tunable Functionality and Improved Sensing Capability. *Nanoscale* **2018**, *10* (37), 17525−17533.
(49) Kim, J. H.; Ko, T.-J.; Okogbue, E.; Han, S. S.; Shawkat, M. S.; Kaium, M. G.; Oh, K. H.; Chung, H.-S.; Jung, Y. Centimeter-scale Green Integration of Layer-by-Layer 2D TMD vdW Heterostructures on Arbitrary Substrates by Water-Assisted Layer Transfer. *Sci. Rep.* **2019**, *9* (1), 1641.
(50) Sebastian, A. R.; Kaium, M. G.; Ko, T.-J.; Shawkat, M. S.; Jung, Y.; Ahn, E. C. Temperature Dependent Studies on Centimeter-scale MoS_2 and vdW Heterostructures. *Nanotechnology* **2022**, *33* (50), 505503.
(51) Islam, M. A.; Li, H.; Moon, S.; Han, S. S.; Chung, H.-S.; Ma, J.; Yoo, C.; Ko, T.-J.; Oh, K. H.; Jung, Y.; et al. Vertically Aligned 2D MoS_2 Layers with Strain-Engineered Serpentine Patterns for High-Performance Stretchable Gas Sensors: Experimental and Theoretical Demonstration. *ACS Appl. Mater. Interfaces* **2020**, *12* (47), 53174−53183.
(52) Dumitru, L. M.; Manoli, K.; Magliulo, M.; Ligonzo, T.; Palazzo, G.; Torsi, L. A Hydrogel Capsule as Gate Dielectric in Flexible Organic Field-Effect Transistors. *APL Mater.* **2014**, *3* (1), 014904.
(53) Chen, D.; Li, J.; Wei, Z.; Wei, X.; Zhu, M.; Liu, J.; Zhang, G.; Zhang, Z.; Chen, J.-H. Repairable Polymer Solid Electrolyte Gated MoS_2 Field Effect Devices with Large Radiation Tolerance. *Adv. Electron. Mater.* **2022**, *8* (1), 2100619.
(54) Wu, Y.; Ringe, S.; Wu, C.-L.; Chen, W.; Yang, A.; Chen, H.; Tang, M.; Zhou, G.; Hwang, H. Y.; Chan, K.; et al. A Two-Dimensional MoS_2 Catalysis Transistor by Solid-State Ion Gating Manipulation and Adjustment (SIGMA). *Nano Lett.* **2019**, *19* (10), 7293−7300.
(55) Alam, M. H.; Xu, Z.; Chowdhury, S.; Jiang, Z.; Taneja, D.; Banerjee, S. K.; Lai, K.; Braga, M. H.; Akinwande, D. Lithium-ion Electrolytic Substrates for Sub-1V High-performance Transition Metal Dichalcogenide Transistors and Amplifiers. *Nat. Commun.* **2020**, *11* (1), 3203.
(56) Liu, N.; Chen, R.; Wan, Q. Recent Advances in Electric-Double-Layer Transistors for Bio-Chemical Sensing Applications. *Sensors* **2019**, *19*, 3425.
(57) Kim, E.; Kim, M. H.; Song, J. H.; Kang, C.; Park, W. H. Dual Crosslinked Alginate Hydrogels by Riboflavin as Photoinitiator. *Int. J. Biol. Macromol.* **2020**, *154*, 989−998.
(58) Draget, K. I.; Skjåk-Bræk, G.; Christensen, B. E.; Gåserød, O.; Smidsrød, O. Swelling and Partial Solubilization of Alginic Acid Gel Beads in Acidic Buffer. *Carbohydr. Polym.* **1996**, *29* (3), 209−215.
(59) Roger, S.; Talbot, D.; Bee, A. Preparation and Effect of Ca^{2+} on Water Solubility, Particle Release and Swelling Properties of Magnetic Alginate Films. *J. Magn. Magn. Mater.* **2006**, *305* (1), 221−227.
(60) Davidovich-Pinhas, M.; Bianco-Peled, H. A Quantitative Analysis of Alginate Swelling. *Carbohydr. Polym.* **2010**, *79* (4), 1020−1027.
(61) Tsai, L.; Stadtman, E. R. Riboflavin Degradation. *Methods in Enzymology*; Academic Press, 1971; Vol. *18*, pp 557−571.
(62) Yoo, C.; Kaium, M. G.; Hurtado, L.; Li, H.; Rassay, S.; Ma, J.; Ko, T.-J.; Han, S. S.; Shawkat, M. S.; Oh, K. H.; et al. Wafer-Scale Two-Dimensional MoS_2 Layers Integrated on Cellulose Substrates Toward Environmentally Friendly Transient Electronic Devices. *ACS Appl. Mater. Interfaces* **2020**, *12* (22), 25200−25210.
(63) Yoo, C.; Yoon, J.; Kaium, M. G.; Osorto, B.; Han, S. S.; Kim, J. H.; Kim, B. K.; Chung, H.-S.; Kim, D.-J.; Jung, Y. Large-area Vertically Aligned 2D MoS_2 Layers on TEMPO-cellulose Nanofibers for Biodegradable Transient Gas Sensors. *Nanotechnology* **2022**, *33* (47), 475502.
(64) Deokar, G.; Vignaud, D.; Arenal, R.; Louette, P.; Colomer, J. F. Synthesis and Characterization of MoS_2 Nanosheets. *Nanotechnology* **2016**, *27* (7), 075604.
(65) Xu, L.; Zhang, Y.; Feng, L.; Li, X.; Cui, Y.; An, Q. Active Basal Plane Catalytic Activity via Interfacial Engineering for a Finely Tunable Conducting Polymer/MoS_2 Hydrogen Evolution Reaction Multilayer Structure. *ACS Appl. Mater. Interfaces* **2021**, *13* (1), 734−744.
(66) Wang, T.; Zhuo, J.; Du, K.; Chen, B.; Zhu, Z.; Shao, Y.; Li, M. Electrochemically Fabricated Polypyrrole and $MoS_{<i>x</i>}$ Copolymer Films as a Highly Active Hydrogen Evolution Electrocatalyst. *Adv. Mater.* **2014**, *26* (22), 3761−3766.
(67) Babuska, T. F.; Curry, J. F.; Dugger, M. T.; Lu, P.; Xin, Y.; Klueter, S.; Kozen, A. C.; Grejtak, T.; Krick, B. A. Role of Environment on the Shear-Induced Structural Evolution of MoS_2 and Impact on Oxidation and Tribological Properties for Space Applications. *ACS Appl. Mater. Interfaces* **2022**, *14* (11), 13914−13924.
(68) Singh, R.; Rathore, D.; Pandey, C. M.; Geetanjali; Srivastava, R. Electrochemical and Spectroscopic Studies of Riboflavin. *Anal. Chem. Lett.* **2018**, *8* (5), 653−664.
(69) Ghim, D.; Chou, P. I.; Chae, S. H.; Jun, Y. S. Effects of MoS_2 Layer Thickness on Its Photochemically Driven Oxidative Dissolution. *Environ. Sci. Technol.* **2021**, *55* (20), 13759−13769.
(70) Rivas Aiello, M. B.; Romero, J. J.; Bertolotti, S. G.; Gonzalez, M. C.; Mártire, D. O. Effect of Silver Nanoparticles on the Photophysics of Riboflavin: Consequences on the ROS Generation. *J. Phys. Chem. C* **2016**, *120* (38), 21967−21975.

https://doi.org/10.1021/acsami.4c09275
ACS Appl. Mater. Interfaces 2024, 16, 39673−39682